Article

Disposable Optical Stretcher Fabricated by Micro Injection Moulding

G. Trotta[1], R. Martínez Vázquez[2]*, A. Volpe[3], F. Modica[1], A. Ancona[3], I. Fassi[4], R. Osellame[2]

[1] *STIIMA CNR, Institute of Intelligent Industrial Technologies and Systems for Advanced Manufacturing, National Research Council, Bari, Italy;*

[2] *IFN CNR, Institute for Photonics and Nanotechnologies, National Research Council, Milan, Italy;*

[3] *IFN CNR, Institute for Photonics and Nanotechnologies, National Research Council, Bari, Italy;*

[4] *STIIMA CNR, Institute of Intelligent Industrial Technologies and Systems for Advanced Manufacturing, National Research Council, Milan, Italy.*

**Correspondence: rebeca.martinez@polimi.it*

Abstract: Micro Injection molding combined with the use of removable inserts is one of the most promising manufacturing process for microfluidic devices, such as Lab-on-a-chip, that have the potential to revolutionize the healthcare and diagnosis system. In this work we have designed, fabricated and tested a compact and disposable plastic optical stretcher. To produce the mould inserts, two micro manufacturing technologies have been used. Micro Electro Discharge machining was used to reproduce the inverse of the capillary tube connection characterized by high aspect ratio. Thanks to the high accuracy of femtosecond laser machining, instead, we manufactured insert with perfectly aligned microfluidic channels and fiber slots, facilitating the final composition of the optical manipulation device. The optical stretcher operation is tested using microbeads and red blood cells solutions. The prototype presented in this work demonstrates the feasibility of this approach that should guarantee a real mass production of ready-to-use- Lab-on-a-chip.

Keywords: microfluidics; micro-injection-moulding; femtosecond laser micromachining; optical manipulation.

1. Introduction

The development of simple and miniaturized Lab-on-Chip (LoC) devices, able to perform analysis on very small volumes of biological samples through optical or electrical probes, is a growing and interdisciplinary field that will help to improve the comprehension of basic biological mechanisms, above all when the analysis are performed at single cell level [1,2]. In particular, several results reported in the scientific literature demonstrate that single cell mechanical properties are reliable markers of a specific cell status [3].

An optical stretcher is based on the exploitation of optical forces to study the viscoelastic properties of individual cells, and it represents an accurate, non-invasive and gentle manipulation technique. In the integrated optical stretcher, an individual cell (flowing inside a microfluidic channel) is trapped between two divergent, opposing laser beams. A stress is exerted on the cell where the light hits the surface causing an elongation of the cell body along the laser beam axis (stress-strain elasticity experiment) [4]. The development of disposable devices for single cell analysis

Peer-reviewed version available at Micromachines 2018, 9, 388; doi:10.3390/mi9080388

will pave the way for it massive exploitation in laboratories as a tool for early diagnosis of diseases [5].

Traditional approaches to LoC fabrication largely rely on the use of conventional inorganic substrates, such as silicon and glass [6,7]. Due to the need for practical low-cost and disposable devices, these materials are being gradually replaced with polymeric substrates, such as thermoplastic poly(methyl methacrylate) (PMMA), which have good optical properties that are crucial for the realization of optofluidic devices.

Khoury Arvelo et al. [8] introduced a low-cost, all-polymer microfluidic chip with integrated DUV-induced waveguides which serves as a platform for optical manipulation of microbeads in a liquid flow. The all-polymeric microfluidic chip consists of two PMMA parts sealed together: the substrate with the microfluidic channel and waveguides, and the lid with holes for fluidic access. The substrate of the chip is fabricated in two steps: hot embossing of the microfluidic channel and waveguide photo-induction.

De Coster et al. [9] proposed a novel polymer microfluidic device with integrated particle manipulation in which fiber-optic laser beams are used to optically trap particles in a microchannel. The robust chip, made of PMMA, is obtained due to the design of the chip and the use of double-sided hot embossing.

Matteucci et al. [10] presented a chip successfully produced in hard cyclic olefin copolymer (CoC) TOPAS 5013 by injection molding based on a Nickel shim with a multi-layer structure used as experimental setups for optical stretching.

The increasing interest in microfluidic devices for healthcare and diagnostics applications has pushed the research to evaluate alternative manufacturing technologies that can reduce the production costs and guarantee a mass production of ready-to-use micro structured devices [11]. In the last years, micro injection moulding (μIM) has become one of the most promising technologies for the production of such kind of devices thus attracting great interest from researches, as witnessed by the numerous reviews published [12-14]. It requires the fabrication of moulds and tools which is typically the weak point of the technology since those elements are quite expensive and limit the re-configurability of the device layout.

However, the increasing difficulties in terms of number of functionalities presented in a single device require a technological upgrade of the micro injection molding process, an upgrade that guarantees, not only a high level of replicability of the devices themselves, but also the need for flexibility to be able to make improvements on ongoing features.

In this direction, the mould becomes a real micro-manufacturing laboratory in which different design strategies and micro manufacturing techniques are experimented to achieve the required level of precision and versatility.

In this work, we use a novel variation of microinjection molding of PMMA introducing the concept of removable and tailored inserts, structured by high-resolution femtosecond laser micromachining (FLM) and micro Electro Discharge machining (μ-EDM) [15]. FLM is able to process, with high removal rate, large surface areas with relatively small depth features, providing precision and surface roughness satisfying the specific requirements of the microfluidic application [16]. μ-EDM, instead, is the leader technology for high aspect ratio geometries due to the small removal rate together with a fine pulse discharge that ensures high precision and good surface roughness also on the walls [17]. The obtained PMMA slabs will be afterwards bonded with the femtosecond laser [18], avoiding

Preprints (www.preprints.org) | NOT PEER-REVIEWED | Posted: 9 July 2018 doi:10.20944/preprints201807.0133.v1

Peer-reviewed version available at Micromachines 2018, 9, 388; doi:10.3390/mi9080388

problems related to thermal or glue bonding. The flexibility of this approach allows us to change the scheme of the microfluidic chip fast and cost effectively.

To prove its feasibility, we present, and validate, a single cell manipulator (an optical stretcher) which turned out to be an excellent example of disposable device because it is cheap, easy to fabricate and to align. We demonstrate its working principle by trapping and stretching red blood cells (RBC).

2. Device and μIM mould design

2.1. Optical stretcher design

In Fig. 1 is reported the design of the optical stretcher defined taking under consideration the monolithic previous version reported in [7]. The device is composed of two shells, both of 19.5 mm length, 7.5 mm large and 0,7 mm thick. The lower shell contains the main microfluidic features: a microchannel of 100 μm depth and 90 μm width, reservoirs of 1 mm diameter and V-grooves for laser fiber housing with 180 μm depth and 235 μm width. The upper shell closes the microfluidic chip and works as the interface with the external peristaltic pressure pump, through two capillary tubes connected to the capillary tubes housing. With respect to the original design [7], where the coaxial connectors were glued at the top of the upper shell, the updated design foresees a direct fabrication of the connectors on the upper shell (Fig. 1), thus reducing the number of external components involved in the assembly. Moreover, a smoothest area in the center was realized in order to allow a good imaging of the specimens flowing inside the microchannel. The shells have been bonded using the femtosecond laser welding approach reported in [18].

The polymer PMMA (Acyrex CM211) has been selected as material for the device fabrication due to its characteristic properties such as mechanical strength, optical transparency, chemical stability and biocompatibility.

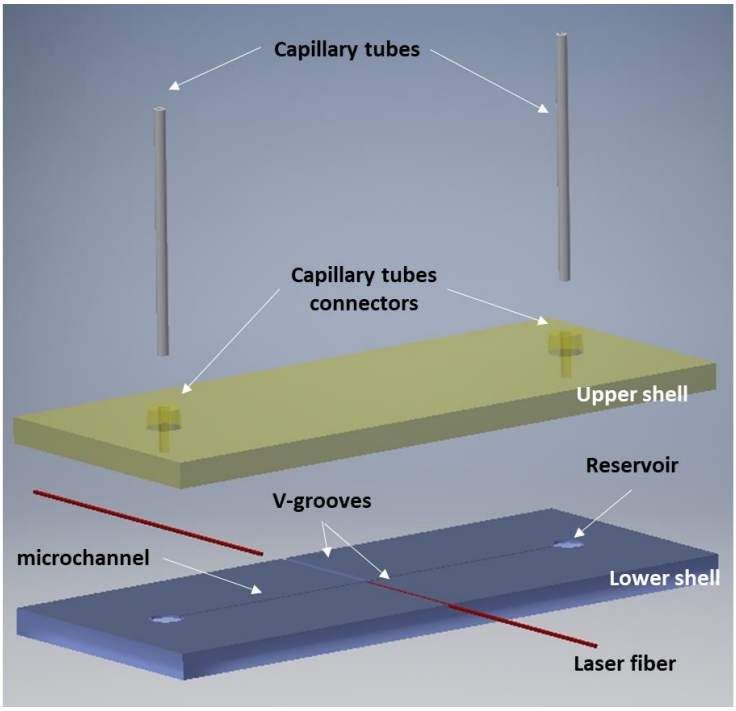

Figure 1. Design of the optical stretcher.

Peer-reviewed version available at Micromachines 2018, 9, 388; doi:10.3390/mi9080388

2.2. *Micro injection moulding*

The numerical simulation of micro injection moulding process with Autodesk Moldflow Insight® has been used to define the final device design and to identify the right runner and gate design in order to avoid incomplete filling of the shell, while facilitating the separation from the final component without damaging it.

A 3D fine mesh (Fig. 2 a and b) has been used to reach sufficient contour accuracy [19]. The bias ratio through thickness was not set as suggested in [20] because the thin plate proposed in this work has no variation in thickness geometry and this condition is helpful to reduce computation time.

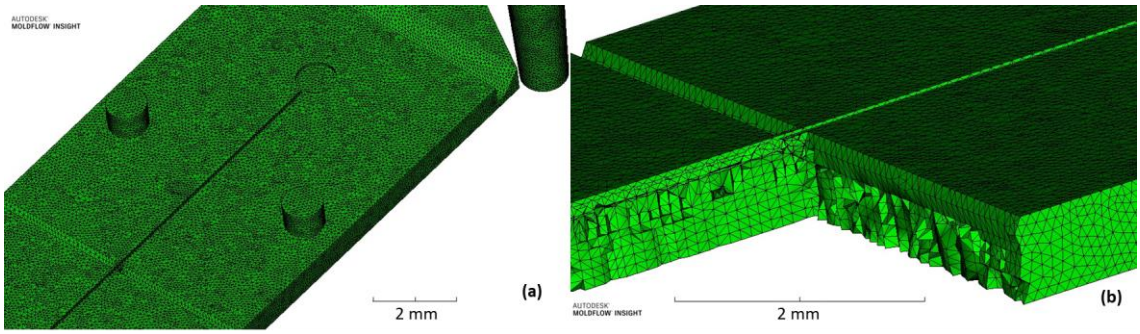

Figure2. a) Overview of mesh size (fine mesh at 100 μm with merge tolerance 10 μm) and b) 3D mesh with number of element trough thickness (10 elements).

The identification of the best process parameters have followed the methodology introduced in Trotta et al. [21] and already tested by Martínez Vázquez et al. [15]. The filling behavior has been analyzed in order to verify that the complementary geometries of the plastic part (sprue, runner and gate) do not interfere with the filling of the fluid by creating areas of hesitation or flow overlapping. As we can see in Fig. 3 a, the melt flow accelerates along the fan-gate, as expected, and then it is uniformly distributed along the whole component without hesitation effects. A second parameter analyzed was the volumetric shrinkage. It allows to estimate the tension distribution in the material so that the warpage effect is reduced together with the deflection in plane of the part [19]. As shown in Fig 3b, the average volumetric shrinkage is between 2÷4 %, as suggested by material datasheet, and the evaluation of the thin plate deflection (Fig. 3c) in the Z direction (out of XY plane) is of few microns and it is localized in the last part of the component, just where the volumetric shrinkage is higher than in the rest of the component.

Preprints (www.preprints.org) | NOT PEER-REVIEWED | Posted: 9 July 2018 doi:10.20944/preprints201807.0133.v1

Peer-reviewed version available at Micromachines 2018, 9, 388; doi:10.3390/mi9080388

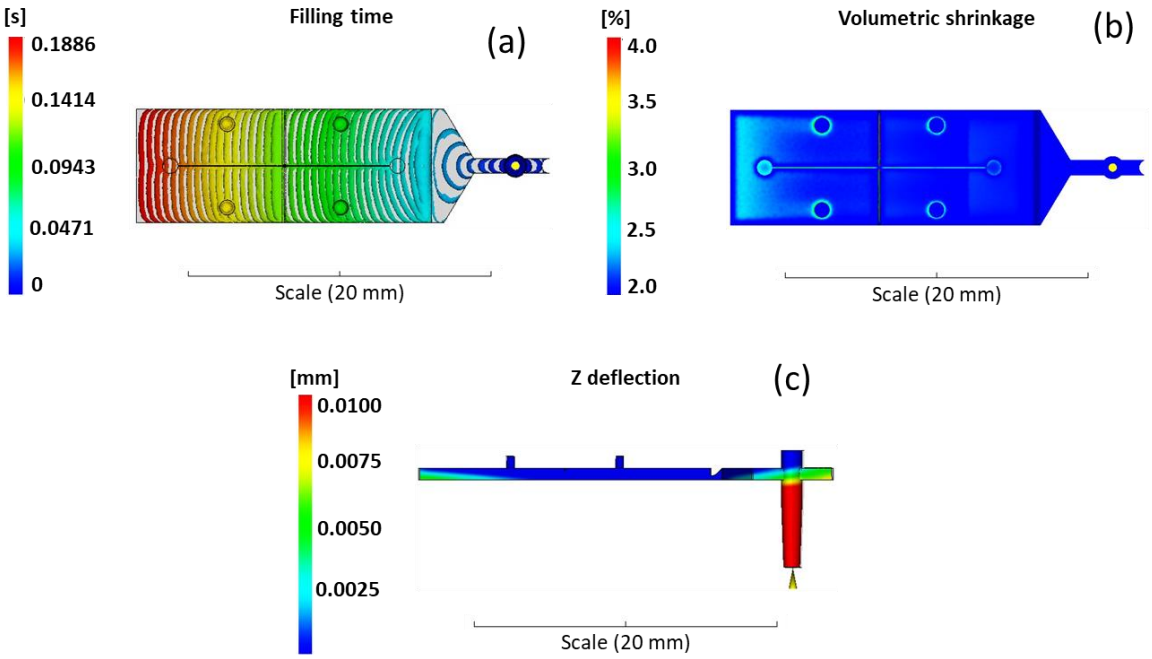

Figure 3. (a) Polymer filling distribution (time contour plot), (b) volumetric shrinkage (range 2%-4%), and (c) component deflection in the Z direction (out of XY plane).

A set of process parameters that meet the criteria described above has been identified with simulations and reported in Table 1 where: T_{melt} (melt temperature), T_{mould} (mould temperature), V_{inj} (injection speed), P_{hold} (packing pressure), t_{hold} (packing time), t_{cool} (cooling time) and Run (plunger injection run).

Table 1. Values for the microinjection moulding process parameters obtained from the simulations.

Material	T_{melt} [°C]	T_{mould} [°C]	V_{inj} [mm/s]	P_{hold} [bar]	t_{hold} [s]	t_{cool} [s]	Run [mm]
PMMA	250	80	100	1000	5	5	18

The design of the mould and of the tailored inserts (Fig. 4a) aimed to satisfy the request of flexibility necessary to target the desired functionalities. The mold has been conceived as an assembly of interchangeable inserts, each one used for a functionality [15]. The two cavities related to the two shells have been designed symmetrically on two identical and interchangeable inserts (Fig. 4b-c). Within the insert, other smaller ones have been placed to realize, for example, the housing for the capillary tubes (Fig. 4d).

Peer-reviewed version available at Micromachines 2018, 9, 388; doi:10.3390/mi9080388

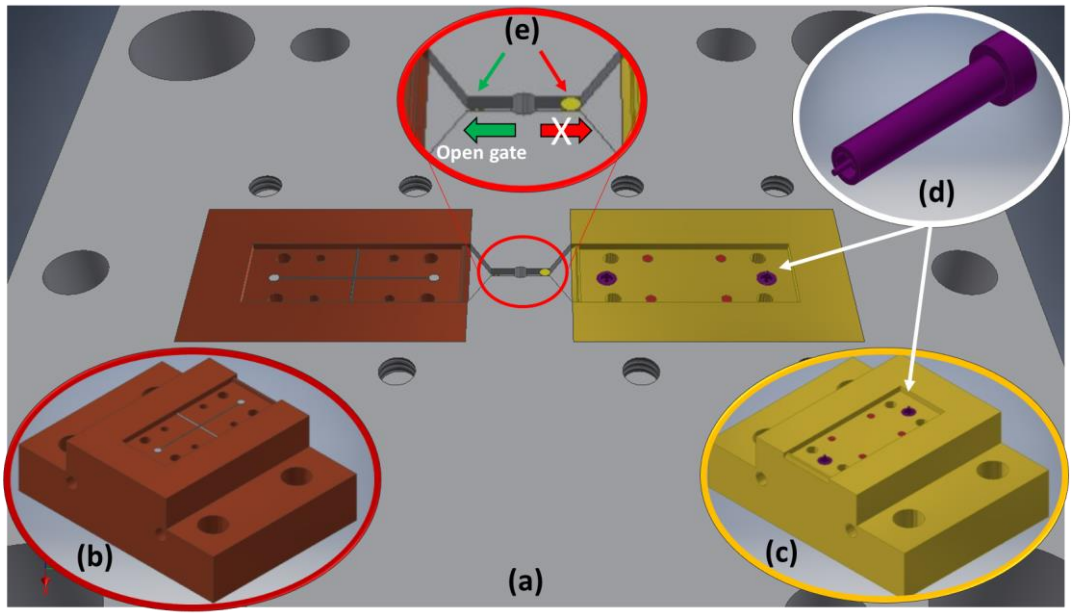

Figure 4. (a) Design of the mould plate with runners and gates (a), (b)(c) main features inserts and (d) small inserts for capillary tube connectors and (e) overview of the interchangeable pins to alternatively close a runner while feeding the other.

This design methodology has provided a considerable versatility to the mould because each micro feature could be easily replaced independently of the others simply replacing the related insert with the new one (Fig. 4b and 4c). Furthermore, the strategy to realize a double symmetric gate together with a single sprue on the same plate facing the inserts with cavities was adopted (Fig 4a and 4e). In this way, the cavities are independent from the feeding system and therefore easily changeable. A further element that guarantees greater flexibility to the process in terms of maximum injectable volume usable for each cavity, as seen in [15], has been adopted also in this case and consists of a couple of interchangeable pins having different height. They could be used alternatively to close a runner while the other one is open (Fig.4e) so that one cavity at a time is fulfilled.

3. Fabrication

3.1. Inserts manufacturing

The master mould and the "bulk" inserts have been fabricated with conventional manufacturing technologies such as milling and die sinking (Fig. 5a) and then assembled to test the tolerances. Then the inserts (Fig. 5b) have been manufactured following two different strategies: the insert with microfluidic features (microchannel, reservoirs and V-grooves) have been fabricated with FLM, instead the insert with the inverse of the upper shell, with smoothest area in the center and the inverse of the capillary tube housing inserts, have been manufactured by μEDM technology.

Peer-reviewed version available at Micromachines 2018, 9, 388; doi:10.3390/mi9080388

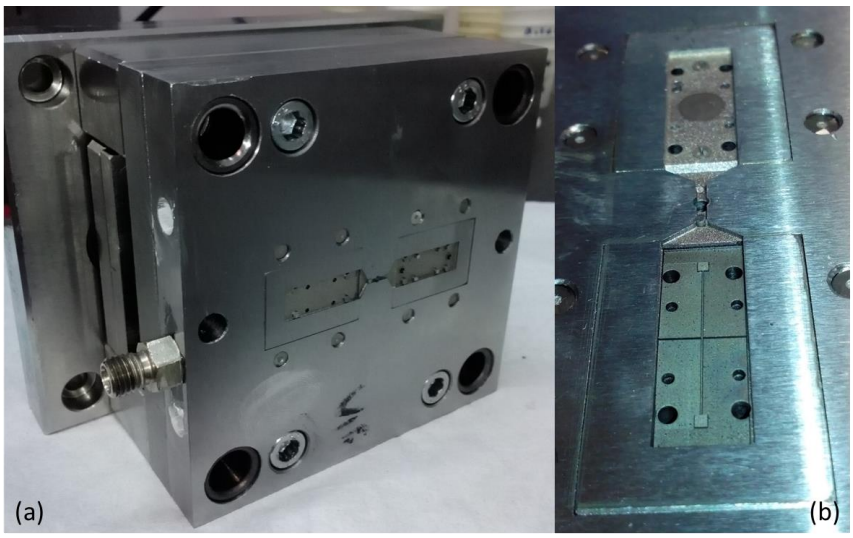

Figure5. (a) Overview of the master mould and (b) of the inserts machined with FLM and μEDm technologies.

3.1.1. FLM

For FLM, we used an ultrafast fiber laser amplifier from Active Fiber Systems GmbH (Jena, Germany) based on the chirped pulse amplification technique (CPA). The laser source delivered an almost diffraction-limited beam (M^2 ~1.25) at a wavelength of 1030 nm with a pulse duration in the range of 650 fs to 20 ps, a repetition rate varying from 50 kHz to 20 MHz, a maximum average power of 50 W, or a maximum pulse energy of 100 μJ.

The linearly polarized beam exiting from the laser source was firstly converted into circularly polarized light by a quarter-wave-plate and then focused and moved onto the target surface through a galvo-scan head (model Hurryscan from SCANLAB GmbH, Puchheim, Germany) equipped with a F-theta lens of 100 mm focal length. The resulting beam spot size on the metal surface was about 20 μm. The fs-laser milling process has been carried out by removing the material layer by layer, by alternating overlapped vertical and horizontal hatch patterns of the laser beam onto the target surface. The ablation depth of the micro-milled area was finely controlled with micrometer precision by adjusting the number of scanning loops without affecting the surface quality.

After milling process, the specimens were ultrasonically cleaned with isopropanol for 10 min to remove the redeposited debris. The ablation depth and the features dimensions were measured by a confocal microscopy Zeiss Axio CSM 700 using a 10X lens. The roughness measurement were realized with the confocal microscopy using a 100X lens for a sample length of 08 mm. The calculation of the roughness is based on the DIN EN ISO 4287 standard. The best measured average surface roughness (Ra) was 0,59 μm and it has been performed at a laser repetition rate of 50 kHz, with a power of 400 mW and 7.05 TW/cm^2 peak intensity, at the focus of the F-theta lens moving the beam at a speed of 600 mm/s with a separation between adjacent scanned lines of 2 μm. Set these parameters, the main dimensions of the features obtained are reported in Fig. 6 and are in line with the expected values reported in Section 2.1.

Preprints (www.preprints.org) | NOT PEER-REVIEWED | Posted: 9 July 2018 doi:10.20944/preprints201807.0133.v1

Peer-reviewed version available at Micromachines 2018, 9, 388; doi:10.3390/mi9080388

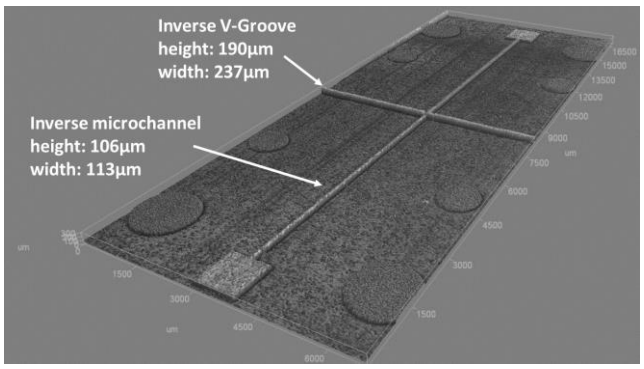

Figure 6. Machined 'inverse' microchannel and V-grooves main dimensions measured with confocal microscope Zeiss Axio CSM 700 (magnification 10X with NA 0.25, lateral digital resolution of 160 nm and vertical resolution of 0.5 µm).

3.1.2. µEDM

On the upper shell insert of Fig. 7a are visible the small inserts for creating the capillary tube connectors. Main features dimensions are illustrated in Fig. 7b and are indicative of the manufacturing complexity due to the micro size and to the slander and conical shapes. Thanks to low energy discharge and high accuracy, µ-EDM process has been adopted for inserts fabrication.

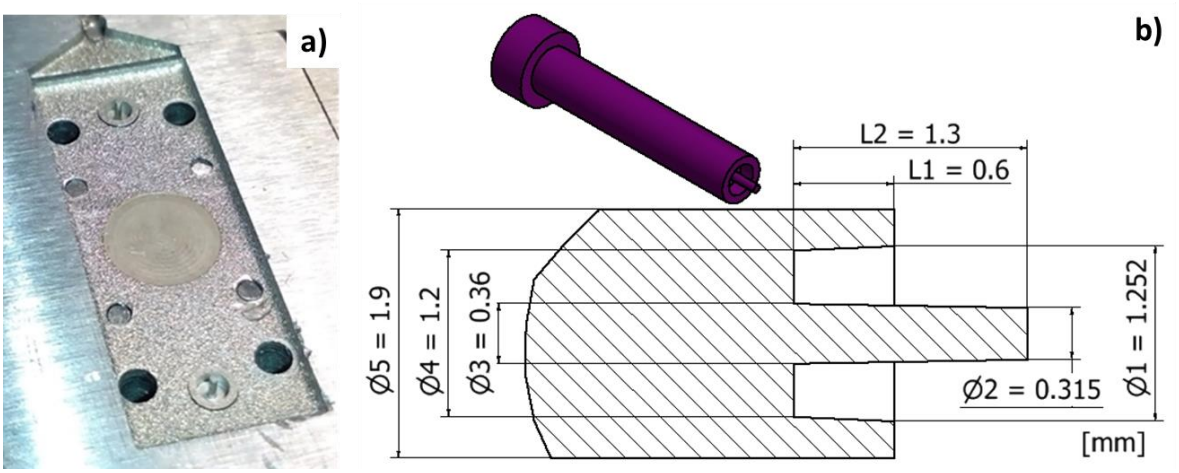

Figure 7. a) Overview of the µEDM inserts with the capillary tube housing inserts and central circle machined with low roughness and b) main dimensions of the capillary tube housing insert.

Starting from a cylindrical workpiece, assembled and referred to the main mold, the central conical pin was obtained by eroding the cavities following two operations. In the first operation, an electrode tool made of tungsten carbide (WC-Co) and having a diameter of 0.4 mm was adopted for reducing the cylindrical diameter and obtaining the first 0.7mm of the conical pin. In order to reduce the machining time, the energy level used was that for semi-roughing regime. Since µ-EDM milling was implemented in a layer-by-layer strategy, a layer thickness of 0.004 mm was chosen to obtain a smooth surface and avoid step-like effects. The machining time for this first operation was 45 min corresponding to a Material Removal Rate (MRR) of 0.064 mm³/min. The second operation required

the use of a smaller WC electrode tool, having a diameter of 0.15 mm, in order to machine the narrow cavity floor at the pin root. In order to prevent tool breakage (due to its small size) the spark energy level used in this machining step was that of a finishing regime with a layer thickness of 0.0012mm. This operation started by eroding the cavity beginning from a depth of 0.7 mm and proceeded until the final conical pin profile was completed at a depth of 1.3 mm. This second operation was concluded in 11 hours and 5 minutes producing a MRR of 0.001 mm^3/min. It must be underlined that being the two operations performed using two different machining regimes, different surface qualities were obtained: Ra = 0.9 µm for semi-roughing regime and Ra=0.6 µm for finishing regime, respectively. The difference between these two surface quality values has been evaluated as acceptable.

3.1.3. uIM shells manufacturing

The micro injection moulding machine used for the part manufacturing was the DESMA Tec Formica Plast 1K, a machine properly developed for micro injection moulding, characterized by a very small plunger (3mm^2), a maximum injection volume of 150 mm^3 and an injection speed up to 500 mm /sec.

The set of process parameters identified with simulation, and reported in Table 1, has been used to produce the two shells of the optical stretcher without significant adjustments, as already highlighted in [21].

In Fig. 8a and b the PMMA lower shell, with the microchannel and the V-grooves, and the PMMA upper shell, with the capillary tube connectors and smooth circle surface, are visible.

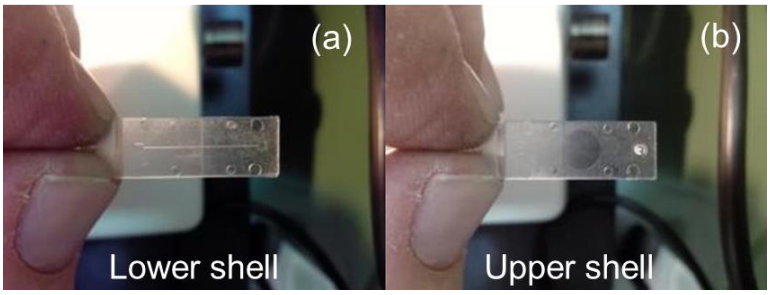

Figure 8. PMMA lower (a) and upper shells (b) of the LoC prototype.

4. Optical stretcher demonstration

The final plastic optical stretcher consisted of a central channel and two closing ducts that will hold the optical fibers. No separation wall was present between the ducts and the microfluidic channel in order to avoid its damaging due to infrared light absorption during the trapping and stretching experiments. The fiber ducts were mutually aligned in order to ensure that the two counter propagating beams were perfectly super positioned at a 20µm depth with respect to the channel floor. In this position, the optical trap intercepted the maximum number of particles. A picture of the final device is shown in Fig. 9, with the peek tubes and the optical fibers inserted in their respective

positions. The trace of the laser bonding around the microfluidic channel and ducts is clearly visible. In order to have a perfectly closed, robust and portable device once the fibers were inserted in their ducts, they were glued with an UV curing glue (Norland Products Inc.).

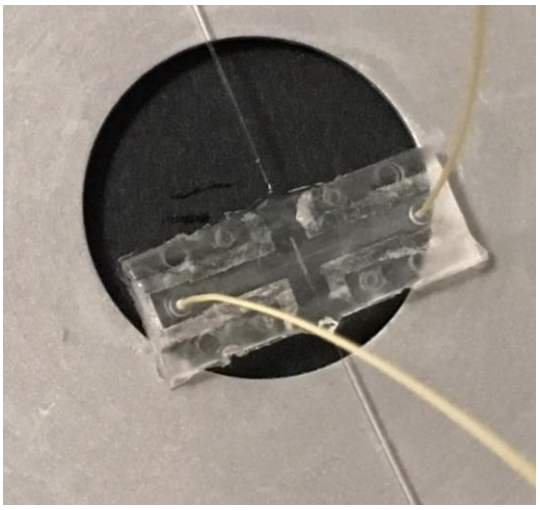

Figure 9. Picture of the final plastic optical stretcher with the peek tubes (yellow) and optical fibers inserted in it.

A preliminary inspection of the device under the microscope evidenced a channel roughness too high to avoid good phase contrast imaging. A chloroform vapor treatment was used in order to improve the transparency of the channel following the procedure reported by DeMarco et al. [22]. Figure 10 shows the microscope images of channels treated with different chloroform vapor exposures times. The flowing polystyrene beads allowed to better capture the improvement in the imaging inside the channel from the pristine one (a) to the 4 minutes treated one (c). It is worth noticing that an overexposure (6 minutes) started to damage the channel surface.

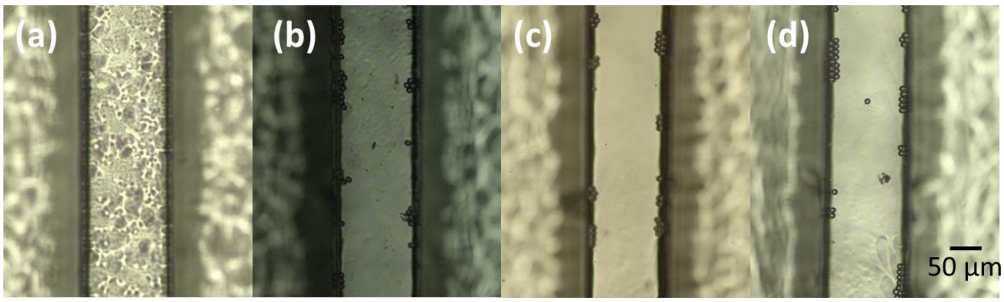

Figure 10 . Microscope images of PMMA microinjected channels with no chloroform treatments (a) and with exposures times of b) 2 minutes, c) 4 minutes and d) 6 minutes.

For the device demonstration a traditional optical stretcher setup was used. The laser source was a continuous wave ytterbium fiber laser (YLD-5k-1070, IPG Fibertech) emitting up to 5 mW at 1070nm. The output beam was split into two single mode fibers 8HI-1060-Corning) by a 50%-50% fiber coupler. The chip was mounted on to a phase contrast inverted microscope (Leica) to capture the particles flowing, trapped and stretched in the microfluidic channel. The phase contrast images

were acquired by a CCD camera (DFC310 FX, Leica) through a bandpass optical filter that cuts the infrared light (FGS550, Thorlabs) [6].

A preliminary test was done inserting a solution of polystyrene microbeads (7μm diameter) inside the microfluidic channel. It was possible to trap the micro-beads with less than 7 μW laser power on each branch. In Fig. 11 there are shown the phase contrast microscope images of a trapped bead with the IR filter inserted or not, in order to demonstrate that the bead was trapped due to the light beams out coming from the crossing optical fibers.

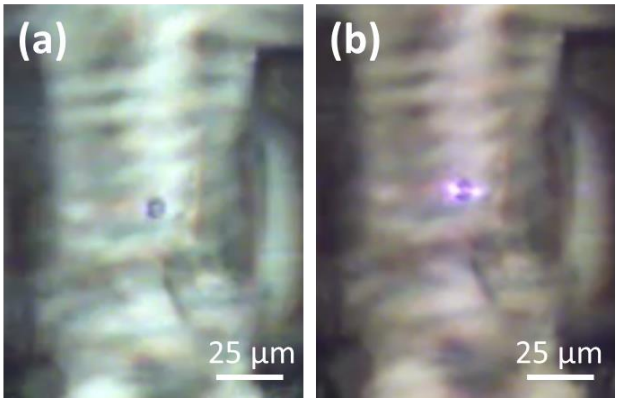

Figure 11. Image of a trapped polystyrene bead (7μm diameter) with the IR light filter on (a) and off (b). The scattering on both sides of the bead demonstrates the trapping due the light out coming from the optical fibers.

The final trapping and stretching test was done using red blood cells (RBC). In order to obtain a sample of quasi-spherical RBCs with 8μm diameter, we diluted 10μL of blood in 8 mL of hypotonic solution.

At flowing speeds in the range between 10 to 50 μL/s RBC, trapping was achieved with an estimated optical power out coming from each fiber of 30mW. Once a single cell was trapped, it could be stretched increasing the optical power out coming from the fibers, as reported in Figure 12. The stretched RBC shown was suffering a 40% elongation of its diameter with an out coming power of 90mW from each fiber. In the same image it is visible a no-trapped RBC flowing inside the channel.

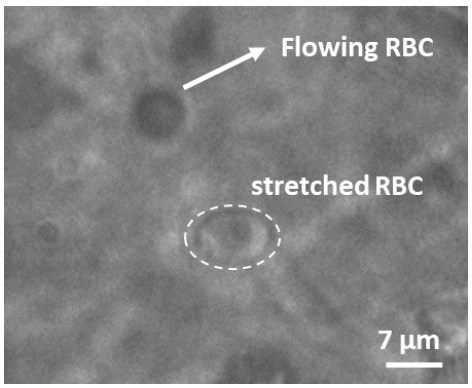

Figure 12 . Phase contrast microscope image of a trapped and stretched RBC (on the background it is visible a flowing RBC).

5. Conclusions

We have reported the design and manufacturing improvements of a PMMA Lab-on-Chip for optical manipulation of single cells produced with μIM technology using the interchangeable inserts approach.

The numerical simulation has been used to assess the feasibility of improvements introduced in the original design, such as capillary tube connectors directly integrated in the upper shell, the identifications of criticalities, such as the centering pins that showed a difficulty to eject the part, and to define the appropriate geometry of the cavity, runners and gate.

A modular design of the mould was conceived to exploit the flexibility achievable by the use of replaceable inserts, on which micro features were fabricated by fs-laser milling and μEDM machining. This choice improved the versatility of the manufacturing technique allowing a real mass production of ready-to-use micro devices.

The assembly of the final LoC was direct and easy: after the laser bonding of the two slabs. The capillary tubes and optical fibers were inserted into their dedicated housing, in particular the optical fibers are well aligned when inserted in the fibers ducts.

A validation of the stretching capabilities of the LoC with RBC solutions has been done, paving the way to future family of cheap and disposable single cell stretchers.

Acknowledgments: The authors gratefully acknowledge the Italian Ministry of Education, University and Research (MIUR) for having supported this research activity within the Progetto Bandiera "La Fabbrica del Futuro - Piattaforma Manifatturiera Nazionale", project PLUS

Conflicts of Interest: "The authors declare no conflict of interest."

Author Contributions: Conceptualization, Roberto Osellame; Funding acquisition, Antonio Ancona, Irene Fassi and Roberto Osellame; Investigation, Gianluca Trotta, Rebeca Martínez Vázquez, Annalisa Volpe and Francesco Modica; Supervision, Antonio Ancona, Irene Fassi and Roberto Osellame; Validation, Rebeca Martínez Vázquez; Writing – original draft, Gianluca Trotta, Rebeca Martínez Vázquez and Annalisa Volpe; Writing – review & editing, Gianluca Trotta, Rebeca Martínez Vázquez and Annalisa Volpe

References

1. El-Ali , J;., Sorger, P.K. ; Jensen K.F. Cells on Chips. *Nature* **2006**, 44, 403.
2. De Souza, N. Single-cell methods. *Nat. Methods* **2011**, 9, 35.
3. Lautenschläger, F.; Paschke, S.; Schinkinger, S.; Bruel, A.; Beil, M.; Guck, J. The regulatory role of cell mechanics for migration of differentiating myeloid cells. *Proc Natl. Acad. Sci*. **2009**, 106, 15696-15701.
4. Guck, J. ; Ananthakrishnan, R.; Mahmood, H.; Moon, T. J. ; Cunningham, C. C.; Käs, J. The optical stretcher: a novel laser tool to micromanipulate cells. *J. Biophys* **2001**, 81, 767-784.
5. Chaudhuri, P.K; Warkiani, M.E.; Jing, T.; Lim, C.T. Microfluidics for research and applications in oncology. *Analyst* **2016**, 141, 504-524.
6. Bellini, N.; Vishnubhatla, K.C. ; Bragheri, F.; Ferrara, L.; Minzioni, P.; Ramponi, R.; Cristiani, I.; Osellame, R. Femtosecond laser fabricated monolithic chip for optical trapping and stretching of single cells. *Opt. Express* **2010**, 18, 4679-4688.
7. Bragheri, F.; Ferrara, L.; Bellini, N.; Vishnubhatla, K.C.; Minzioni, P. ; Ramponi, R.; Osellame, R.; Cristiani, I. Optofluidic chip for single cell trapping and stretching fabricated by a femtosecond laser. *J. Biophotonics* **2010**, 3, 234-243.

8. Arvelo, M. K.; Matteucci, M. ; Sorensen, K.T.; Bilenberg, B.; Vannahme, C.; Kristensen, A.; Berg-Sørensen, K. Optical manipulation with two beam traps in microfluidic polymer systems. 20th Microoptics Conference (MOC), Fukuoka, **2015**, pp. 1-2.
9. De Coster, D.; Ottevaere, H.; Vervaeke, M.; Van Erps, J.; Callewaert, M.; Wuytens, P.; Simpson, S. H. ; Hanna, S.; De Malsche, W.; Thienpont, H. Mass-manufacturable polymer microfluidic device for dual fiber optical trapping. *Opt. Express* **2015**, 23, 30991-31009.
10. Matteucci, M.; Triches, M.; Nava, G.; Kristensen, A.; Pollard, M.R.; Berg-Sørensen, K.; Taboryski, R.J. Fiber-Based, Injection-Molded Optofluidic Systems: Improvements in Assembly and Applications. *Micromachines* **2015**, 6, 1971-1983.
11. Abgrall, P.; Guè, A.M. Lab-on-chip technologies: making a microfluidic network and coupling it into a complete microsystem - a review. *J. Micromech. Microeng.* **2007**, 17 , R15–R49.
12. Attia, U.M. et al. Micro-injection moulding of polymer microfluidic devices. *Microfluid Nanofluid* **2009**, 7, 1–28.
13. Heckele, M. et al. Review on micro molding of thermoplastic polymers. *J. Micromech. Microeng*. **2004**, 14, R1–R14.
14. Dieudonne, A.M. et al. Injection molded microfluidic chips featuring integrated interconnects. *Lab Chip* **2006**, 6, 1346–1354.
15. Martínez Vázquez, R.; Trotta, G.; Volpe, A.; Bernava, G.; Basile, V.; Paturzo, M.; Ferraro, P.; Ancona, A.; Fassi, I.; Osellame, R. Rapid Prototyping of Plastic Lab-on-a-Chip by Femtosecond Laser Micromachining and Removable Insert Microinjection Molding. *Micromachines* **2017**, *8*, 328;
16. Wu, P.H.; Cheng, C.W.; Chang, C.P.; Wu, T.M.; Wang, J.K. Fabrication of large-area hydrophobic surfaces with femtosecond-laser structured molds. *J. Micromech. Microeng*. **2011**, 21, 115032.
17. Cao, D.M.; Jiang, J.; Meng. W.J.; Wang, W. Fabrication of high-aspect-ratio microscale Ta mold inserts with micro electrical discharge machining. *Microsyst Technol*. **2007**, 13, 503–510.
18. Volpe, A.; Di Niso, F.; Gaudiuso, C.; De Rosa, A.; Martínez Vázquez, R.; Ancona, A.; Lugarà, P.M.; Osellame, R. Welding of PMMA by a femtosecond fiber laser. *Opt. Express* **2015**, 23, 4114-4124.
19. Costa, F., Tosello, G. and Whiteside, B., 2009. Best practice strategies for validation of micro moulding process simulation. *Proceedings of Polymer Process Engineering Conference.* **2009**, University of Bradford (United Kingdom), Edited by Coates, P., 331-364.
20. Marhöfer, D. M.; Tosello, G.; Hansen, H. N.; Islam, A. Advancements on the simulation of the micro injection moulding process. *Proceedings of the 10th International Conference on Multi-Material Micro Manufacture 4M Association* **2013**, 77-81.
21. Trotta, G.; Ancona, A.; Volpe, A.; Di Niso, F.; Fassi, I. Improving the flexibility of micro injection moulding by exploiting fs-laser micro milling to realize mould inserts with complex 3D microfeatures. *Proceedings of 4M/ICOMM2015* **2015**, 086, 354-357.
22. De Marco, C. ; Eaton, S. M.; Martinez-Vazquez, R.; Rampini, S.; Cerullo, G.; Levi, M.; Turri, S.; Osellame, R. Solvent vapor treatment controls surface wettability in PMMA femtosecond-laser-ablated microchannels. *Microfluid Nanofluid* **2013**, 14, 171–176.